Longitudinal and transverse impedance of an iris in a beam pipe

Hiromi Okamoto*
Lawrence Berkeley Laboratory, Berkeley, California 94720

Shicheng Jiang and Robert L. Gluckstern
Physics Department, University of Maryland, College Park, Maryland 20742

(Received 1 February 1994)

The use of iris loaded cavities to accelerate high current bunched beams makes it important to understand the impedance and wake fields caused by an iris in a beam pipe. In this paper we present a method to calculate both the longitudinal and transverse impedance of a circular iris of radius b and thickness g in a circular beam pipe of radius a for ultrarelativistic particles. An integral equation is derived for the transverse electric field at the junction between the iris and the beam pipe and a variational expression is obtained for the impedance, using the transverse field as a trial function. Accurate numerical results are obtained for the longitudinal and transverse impedances using a trial function with only a few adjustable parameters. By invoking causality we confirm the analytic behavior of the impedances in the complex frequency plane and obtain the corresponding wake functions. We particularly explore the limit $b \to \infty$ to compare with previous studies of the impedance of a circular hole in a transverse metallic plane.

PACS number(s): 29.27.Bd, 41.75.−i, 41.85.−p

I. INTRODUCTION

An intense beam bunch traveling along or near the axis of an iris loaded accelerator structure can be expected to generate large wake fields. These wake fields, which can be either longitudinal or transverse, can cause undesirable forces either within the bunch or from bunch to bunch, which are capable of spreading the bunch or even of causing disruptive instabilities.

As a first step in understanding these wake fields, we consider a beam pipe of arbitrary (constant) cross section in which a single iris of thickness g is located. A point charge Q then travels along the axis, or near the axis, at ultrarelativistic speed ($\beta = 1, \gamma \gg 1$). We then calculate the coupling impedance as a function of frequency, which turns out to be closely related to the Fourier transform of the wake function (which is the wake field a fixed distance s behind Q, averaged over the transit through the iris).

Short distances correspond to high frequency and vice versa. The increasing use of short bunches and the interest in single bunch instabilities makes it important to understand and calculate the coupling impedance at frequencies above the cutoff of the beam pipe.

Let us outline our method of calculating the longitudinal and transverse coupling impedances. For the longitudinal impedance, we consider the charge density of the moving charge to be

$$\rho(x,y,z;t) = Q\delta(x)\delta(y)\delta(z-ct) = Q\delta(x)\delta(y)\frac{1}{2\pi c}\int_{-\infty}^{\infty} d\omega\, e^{j\omega t - jkz}, \quad (1.1)$$

where $k = \omega/c$. The current density can then be written in the frequency domain as

$$J_z(x,y,z;k) = I_0\delta(x)\delta(y)e^{-jkz}, \quad (1.2)$$

where $I_0 = Q/2\pi$ and where we eventually return to the time domain by multiplying by $\exp(j\omega t)$ and integrating over all real ω.

We now use the source current in Eq. (1.2) and solve for the fields it generates by matching solutions to Maxwell's equations in the beam pipe ($|z| \geq g/2$) with outgoing boundary conditions to solutions in the iris region ($|z| \leq g/2$). (The center of the iris is located at $z = 0$ and all surfaces are ideal conductors.) This procedure will be described in detail in Sec. II. The longitudinal impedance is then defined as [1]

$$Z(k) = -\frac{1}{I_0}\int_{-\infty}^{\infty} dz\, E_z(0,0,z;k)e^{jkz}. \quad (1.3)$$

This can be written as a volume integral by using Eq. (1.2). Specifically

$$Z(k) = -\frac{1}{|I_0|^2}\int d^3x\, \boldsymbol{E}(\boldsymbol{x};k)\cdot\boldsymbol{J}^*(\boldsymbol{x};k). \quad (1.4)$$

We then consider the combination

$$|I_0|^2[Z(k)+Z_p^*(k)] = -\int d^3x\, \boldsymbol{E}(\boldsymbol{x};k)\cdot\boldsymbol{J}^*(\boldsymbol{x};k) - \int d^3x\, \boldsymbol{E}_p^*(\boldsymbol{x};k)\cdot\boldsymbol{J}(\boldsymbol{x};k), \quad (1.5)$$

where the subscript p denotes the geometry with the

*On leave from Institute for Chemical Research, Kyoto University, Kyoto 611, Japan.

beam pipe alone (without the iris). Since $Z_p(k)$ is imaginary (in fact it vanishes for $\gamma \to \infty$), Eq. (1.5) gives the increment to the impedance due to the iris. We express $\boldsymbol{J}^*$ and $\boldsymbol{J}$ in Eq. (1.5) in terms of $\boldsymbol{E}$ and $\boldsymbol{E}_p$ by means of Maxwell's equations. Integration by parts then permits us to express the longitudinal impedance as an integral over the surface [2, 3] of the iris:

$$|I_0|^2 Z_{\parallel}(k) = \int_{\text{iris}} dS\ \boldsymbol{n} \cdot \boldsymbol{E}_p^*(\boldsymbol{x};k) \times \boldsymbol{H}(\boldsymbol{x};k), \quad (1.6)$$

where the fields without the iris have only the transverse components

$$\boldsymbol{E}_p = -e^{-jkz}\nabla_\perp \chi_p\ ,\ Z_0 \boldsymbol{H}_p = \boldsymbol{z} \times \boldsymbol{E}_p. \quad (1.7)$$

Here $\boldsymbol{z}$ is the axial unit vector, i.e., $\boldsymbol{z} = (0,0,1)$, and $\chi_p(x,y)$ is constant on the surface of the beam pipe and is consistent with the line charge singularity of Eqs. (1.1) and (1.2). For example, apart from a constant,

$$\chi_p(r,\theta) = -\ln\ r \quad (1.8)$$

for a circular beam pipe. The azimuthal magnetic field H_θ is obtained by field matching, as will be described in Sec. II.

In a similar manner we can obtain the transverse coupling impedance. Starting with the axial dipole drive current

$$J_z = I_0 \delta(y)[\delta(x-\Delta) - \delta(x+\Delta)]\exp(-jkz) \quad (1.9)$$

we can write the transverse impedance as [3]

$$Z_\perp(k) = -\frac{1}{4k\Delta^2|I_0|^2}\int d^3x\ \boldsymbol{E}(\boldsymbol{x};k)\cdot\boldsymbol{J}^*(\boldsymbol{x};k), \quad (1.10)$$

evaluated in the limit of small Δ. As with the longitudinal impedance this can be converted to the surface integral

$$4k\Delta^2|I_0|^2 Z_\perp(k) = \int_{\text{iris}} dS\ \boldsymbol{n}\cdot\boldsymbol{E}_p^*(\boldsymbol{x};k)\times\boldsymbol{H}(\boldsymbol{x};k), \quad (1.11)$$

but in this case $\chi_p(x,y)$ vanishes at the surface of the beam pipe and is consistent with the dipole singularity of Eq. (1.9). For example, apart from a constant,

$$\chi_p(r,\theta) = -\cos\theta\ \left(\frac{1}{r} - \frac{r}{a^2}\right) \quad (1.12)$$

for a circular beam pipe of radius a. Needless to say $\boldsymbol{H}$ in Eq. (1.11) must be obtained for the drive current in Eq. (1.9).

In Sec. II we present general field matching techniques by which we can obtain $\boldsymbol{E}$ and $\boldsymbol{H}$ for both the longitudinal and transverse impedance calculations. In particular we obtain integral equations for the transverse electric field $\boldsymbol{E}_\perp$ in the transverse planes where the beam pipe and iris meet ($z = \pm g/2$). In Sec. III we obtain expressions for the longitudinal and transverse impedances in terms of $\boldsymbol{E}_\perp$ at $z = \pm g/2$. In Sec. IV we show that these impedances can be written in variational form, ensuring good convergence in subsequent numerical calculations. To obtain the variational form it is necessary to use the integral equation to modify the expressions for the impedance. We also expand $\boldsymbol{E}_\perp$ in terms of a complete set in the iris opening and obtain the general form of the impedances via matrix inversion when the complete set is truncated. In Sec. V we show how the result is simplified when the iris thickness vanishes. The calculations are then particularized to a circular beam pipe and iris opening in Sec. VI for the longitudinal impedance and in Sec. VII for the transverse impedance, and numerical results are presented in Sec. VIII, where we show that the results converge rapidly with the matrix order. In Sec. IX we proceed to the limit of large beam pipe radius, so that we can obtain the longitudinal and transverse impedances of a hole in a plate of finite thickness. In Sec. X we examine the implications of causality, obtaining the general behavior of the impedance at low and high frequency as well as the wake function. Finally, in Sec. XI we summarize the results and compare with previous calculations in the literature.

II. GENERAL ANALYSIS FOR THE FIELDS

In our general derivation we consider a beam pipe of arbitrary cross section as well as an iris hole of arbitrary cross section, both homogeneous in the axial direction. The planes involving the iris sidewalls are perpendicular to the beam pipe axis and the origin of our coordinate system is set at the center of the iris hole region. The cross-sectional area of the iris hole is denoted by S_1 while S_2 represents the sidewalls of the iris. We use latin letters as the subscripts of the quantities defined in the pipe region, i.e., $|z| \geq g/2$, and greek letters for those defined in the iris region, i.e., $|z| \leq g/2$.

A. Fields in the pipe region $|z| \geq g/2$

Let us introduce a general expression for the electromagnetic fields in the pipe region. We first write the nth normal mode for the electric fields in this region as $\boldsymbol{e}_n(\boldsymbol{r})$, which is normalized as

$$\int_{S_1+S_2} dS\ \boldsymbol{e}_n \cdot \boldsymbol{e}_{n'} = \delta_{nn'}. \quad (2.1)$$

The corresponding normalized magnetic field is represented as

$$\boldsymbol{h}_n = \boldsymbol{z} \times \boldsymbol{e}_n. \quad (2.2)$$

The source fields are written as outlined in Eq. (1.7),

$$\boldsymbol{E}_\perp^{(s)} = Z_0 \boldsymbol{H}_\perp^{(s)} \times \boldsymbol{z} = A_0 e^{-jkz}\nabla_\perp \chi(\boldsymbol{r}). \quad (2.3)$$

Here Z_0 is the free-space impedance, A_0 is constant, $\boldsymbol{r}$ denotes transverse coordinate, e.g., $\boldsymbol{r} = (x,y)$, and the source-field potential $\chi(\boldsymbol{r})$ satisfies the proper boundary condition on the pipe surface. Note that we now drop the subscript p. The forms of A_0 and χ, of course, depend on which impedance we consider, i.e., longitudinal monopole impedance or transverse dipole impedance. The total field is the superposition of the source fields in Eq. (2.3) and pipe fields which can be expanded as a sum over the normal modes. In the following analysis, we use the

simplified notation ∇ as the transverse gradient operator $\nabla_\perp$. Therefore, the transverse total fields $\boldsymbol{E}_\perp$ and $\boldsymbol{H}_\perp$ in the region $z \geq g/2$ can be expressed as

$$\frac{\boldsymbol{E}_\perp}{A_0} = e^{-jkz}\nabla\chi + \sum_n a_n \boldsymbol{e}_n e^{-j\beta_n(z-g/2)}, \tag{2.4}$$

$$\frac{Z_0\boldsymbol{H}_\perp \times \boldsymbol{z}}{A_0} = e^{-jkz}\nabla\chi + \sum_n \lambda_n a_n \boldsymbol{e}_n e^{-j\beta_n(z-g/2)}, \tag{2.5}$$

where a_n is the constant expansion coefficient and $\lambda_n \equiv Z_0/Z_n$, where Z_n is the impedance of the nth mode. Similarly, the total fields in the region $z \leq -g/2$ are given by

$$\frac{\boldsymbol{E}_\perp}{A_0} = e^{-jkz}\nabla\chi + \sum_n b_n \boldsymbol{e}_n e^{j\beta_n(z+g/2)}, \tag{2.6}$$

$$\frac{Z_0\boldsymbol{H}_\perp \times \boldsymbol{z}}{A_0} = e^{-jkz}\nabla\chi - \sum_n \lambda_n b_n \boldsymbol{e}_n e^{j\beta_n(z+g/2)}, \tag{2.7}$$

where b_n is the constant expansion coefficient. In Eqs. (2.4)–(2.7) the sign of the wave number β_n has been chosen so that only outgoing waves are taken into consideration. We should also note that $\boldsymbol{e}_n$ includes both TM and TE modes.

B. Fields in the iris hole region $|z| \leq g/2$

In the iris region we introduce the orthonormal mode $\boldsymbol{e}_\nu(\boldsymbol{r})$ normalized as

$$\int_{S_1} dS\ \boldsymbol{e}_\nu \cdot \boldsymbol{e}_{\nu'} = \delta_{\nu\nu'}. \tag{2.8}$$

In this region, there exist waves propagating in the positive and negative axial directions simultaneously. Writing the source field potential as $\sigma(\boldsymbol{r})$ and expanding the fields as a sum over normal modes, the transverse total fields in the region $|z| \leq g/2$ can be expressed as

$$\frac{\boldsymbol{E}_\perp}{A_0} = e^{-jkz}\nabla\sigma + \sum_\nu (a_\nu e^{-j\beta_\nu z} + b_\nu e^{j\beta_\nu z})\boldsymbol{e}_\nu, \tag{2.9}$$

$$\frac{Z_0\boldsymbol{H}_\perp \times \boldsymbol{z}}{A_0} = e^{-jkz}\nabla\sigma + \sum_\nu \lambda_\nu (a_\nu e^{-j\beta_\nu z} - b_\nu e^{j\beta_\nu z})\boldsymbol{e}_\nu, \tag{2.10}$$

where a_ν and b_ν are constant and $\lambda_\nu \equiv Z_0/Z_\nu$. Here Z_ν is the impedance of νth mode in the guide within the iris. The source field potential $\sigma(\boldsymbol{r})$, which is different for the longitudinal and transverse impedances, satisfies the proper boundary condition on the iris surface.

C. Field matching

We now match transverse fields in the transverse plane at the position $z = g/2$. We first write the electric field at this position as

$$\frac{\boldsymbol{E}_u}{A_0} = \begin{cases} e^{-jkg/2}\nabla\sigma + \boldsymbol{u} & \text{on } S_1 \\ 0 & \text{on } S_2, \end{cases} \tag{2.11}$$

where $\boldsymbol{u}(\boldsymbol{r})$ is an unknown vector function. Noting that $\boldsymbol{E}_\perp$ must vanish on the iris wall S_2 because of the boundary condition, the field in Eq. (2.4) and $\boldsymbol{E}_u$ are totally continuous at $z = g/2$ and then

$$\boldsymbol{E}_u = \boldsymbol{E}_\perp(z = g/2) \text{ on } S_1 + S_2. \tag{2.12}$$

After substituting Eqs. (2.4) and (2.11) into Eq. (2.12) and multiplying both sides by $\boldsymbol{e}_n$, we perform the surface integration over $S_1 + S_2$ to obtain

$$a_n = u_n + \xi_n e^{-jkg/2}, \tag{2.13}$$

where we have used the orthogonality (2.1) and

$$\xi_n \equiv \int_{S_1} dS\ \nabla(\sigma - \chi)\cdot \boldsymbol{e}_n - \int_{S_2} dS\ \nabla\chi \cdot \boldsymbol{e}_n, \tag{2.14}$$

$$u_n \equiv \int_{S_1} dS\ \boldsymbol{u}\cdot\boldsymbol{e}_n. \tag{2.15}$$

For the field in Eq. (2.9) and E_u, we have

$$\boldsymbol{E}_u = \boldsymbol{E}_\perp(z = g/2) \text{ on } S_1. \tag{2.16}$$

After substitution of Eqs. (2.9) and (2.11) into Eq. (2.16), multiplication by $\boldsymbol{e}_\nu$, and integration over S_1, we have

$$u_\nu = a_\nu e^{-j\beta_\nu g/2} + b_\nu e^{j\beta_\nu g/2}, \tag{2.17}$$

where

$$u_\nu \equiv \int_{S_1} dS\ \boldsymbol{u}\cdot\boldsymbol{e}_\nu. \tag{2.18}$$

We now repeat the analysis at $z = -g/2$. Introducing the unknown vector function $\boldsymbol{v}(\boldsymbol{r})$, we write the electric field at $z = -g/2$ as

$$\frac{\boldsymbol{E}_v}{A_0} = \begin{cases} e^{jkg/2}\nabla\sigma + \boldsymbol{v} & \text{on } S_1 \\ 0 & \text{on } S_2. \end{cases} \tag{2.19}$$

Matching of the fields in Eqs. (2.6) and (2.9) to that in Eq. (2.19) leads to

$$b_n = v_n + \xi_n e^{jkg/2}, \tag{2.20}$$

$$v_\nu = a_\nu e^{j\beta_\nu g/2} + b_\nu e^{-j\beta_\nu g/2}, \tag{2.21}$$

where

$$v_n \equiv \int_{S_1} dS\ \boldsymbol{v}\cdot\boldsymbol{e}_n, \tag{2.22}$$

$$v_\nu \equiv \int_{S_1} dS\ \boldsymbol{v}\cdot\boldsymbol{e}_\nu. \tag{2.23}$$

Equations (2.13), (2.17), (2.20), and (2.21) permit us to write a_n, b_n, a_ν, and b_ν in terms of $\boldsymbol{u}(\boldsymbol{r})$ and $\boldsymbol{v}(\boldsymbol{r})$.

D. Integral equation for u and v

We now match the magnetic fields at $z = g/2$ and $z = -g/2$ on S_1. Specifically, at $z = g/2$ we have, from Eqs. (2.5) and (2.10),

$$\sum \lambda_n a_n \boldsymbol{e}_n = e^{-jkg/2}\boldsymbol{\nabla}(\sigma - \chi) + \sum \lambda_\nu (a_\nu e^{-j\beta_\nu g/2} - b_\nu e^{j\beta_\nu g/2})\boldsymbol{e}_\nu. \tag{2.24}$$

Similarly, at $z = -g/2$, we have

$$\sum \lambda_n b_n \boldsymbol{e}_n = e^{-jkg/2}\boldsymbol{\nabla}(\sigma - \chi) + \sum \lambda_\nu (a_\nu e^{-j\beta_\nu g/2} - b_\nu e^{j\beta_\nu g/2})\boldsymbol{e}_\nu. \tag{2.25}$$

If we now use Eqs. (2.13), (2.17), (2.20), and (2.21) to express all coefficients in terms of $\boldsymbol{u}$ and $\boldsymbol{v}$, we obtain the two integral equations

$$\int_{S_1} dS'\ \boldsymbol{w}^+(\boldsymbol{r}')\cdot \overleftrightarrow{\boldsymbol{K}}^+(\boldsymbol{r}', \boldsymbol{r}) = \boldsymbol{P}^+(\boldsymbol{r}), \tag{2.26}$$

$$\int_{S_1} dS'\ \boldsymbol{w}^-(\boldsymbol{r}')\cdot \overleftrightarrow{\boldsymbol{K}}^-(\boldsymbol{r}', \boldsymbol{r}) = \boldsymbol{P}^-(\boldsymbol{r}), \tag{2.27}$$

where

$$\overleftrightarrow{\boldsymbol{K}}^+(\boldsymbol{r}', \boldsymbol{r}) = \sum_n \lambda_n \boldsymbol{e}_n(\boldsymbol{r}')\boldsymbol{e}_n(\boldsymbol{r}) + j\sum_\nu \lambda_\nu \boldsymbol{e}_\nu(\boldsymbol{r}')\boldsymbol{e}_\nu(\boldsymbol{r})\tan(\beta_\nu g/2), \tag{2.28}$$

$$\overleftrightarrow{\boldsymbol{K}}^-(\boldsymbol{r}', \boldsymbol{r}) = \sum_n \lambda_n \boldsymbol{e}_n(\boldsymbol{r}')\boldsymbol{e}_n(\boldsymbol{r}) - j\sum_\nu \lambda_\nu \boldsymbol{e}_\nu(\boldsymbol{r}')\boldsymbol{e}_\nu(\boldsymbol{r})\cot(\beta_\nu g/2), \tag{2.29}$$

$$\boldsymbol{P}^+(\boldsymbol{r}) = -\sum_n \lambda_n \xi_n \boldsymbol{e}_n(\boldsymbol{r})\cos(kg/2) + j\sum_\nu \zeta_\nu \boldsymbol{e}_\nu(\boldsymbol{r})\sin(kg/2), \tag{2.30}$$

$$\boldsymbol{P}^-(\boldsymbol{r}) = \sum_n \lambda_n \xi_n \boldsymbol{e}_n(\boldsymbol{r})\sin(kg/2) + j\sum_\nu \zeta_\nu \boldsymbol{e}_\nu(\boldsymbol{r})\cos(kg/2). \tag{2.31}$$

Here

$$\zeta_\nu \equiv \int_{S_1} dS\ \boldsymbol{\nabla}(\chi - \sigma)\cdot \boldsymbol{e}_\nu \tag{2.32}$$

and

$$\boldsymbol{u} = \boldsymbol{w}^+ + j\boldsymbol{w}^-,\quad \boldsymbol{v} = \boldsymbol{w}^+ - j\boldsymbol{w}^-, \tag{2.33}$$

where the equations naturally separate into one involving $\boldsymbol{w}^+$, the even (in z) part of $\boldsymbol{u}$ and $\boldsymbol{v}$, and $\boldsymbol{w}^-$, the odd part of $\boldsymbol{u}$ and $\boldsymbol{v}$. It is straightforward to show that $\zeta_\nu = 0$ for TM modes. [See Appendix, Eq. (A16).] For future reference we also define

$$\chi_n \equiv -\int_{S_2} dS\ \boldsymbol{\nabla}\chi\cdot \boldsymbol{e}_n. \tag{2.34}$$

III. IMPEDANCE INTEGRALS

As outlined in Eqs. (1.6) and (1.11), both the longitudinal (monopole) and transverse (dipole) impedance can be defined in terms of the surface integral

$$Z(k) \doteq \frac{1}{C}\int_{\text{on iris}} dS\ \boldsymbol{n}\cdot(\boldsymbol{E}^{(s)*}\times \boldsymbol{H}), \tag{3.1}$$

where $\boldsymbol{n}$ denotes the unit (inward) normal on the beam pipe and iris and the constant parameter C is

$$C = \begin{cases} |I_0|^2 & \text{for the longitudinal impedance} \\ 4k\Delta^2|I_0|^2 & \text{for the transverse impedance.} \end{cases} \tag{3.2}$$

The integral in Eq. (3.1) is performed on the iris surface and can be separated into two parts:

$$Z(k) = Z_1(k) + Z_2(k), \tag{3.3}$$

with

$$Z_1(k) \equiv \frac{1}{C}\int_{S_2} dS\ \boldsymbol{z}\cdot[(\boldsymbol{E}_\perp^{(s)*}\times \boldsymbol{H}_\perp)_{z=-g/2} - (\boldsymbol{E}_\perp^{(s)*}\times \boldsymbol{H}_\perp)_{z=g/2}], \tag{3.4}$$

$$Z_2(k) \equiv \frac{1}{C}\int_{S_3} dS\ \boldsymbol{n}_h\cdot(\boldsymbol{E}_\perp^{(s)*}\times \boldsymbol{H}), \tag{3.5}$$

where we have written the surface of the iris hole as S_3 and $\boldsymbol{n}_h$ is the unit normal on S_3. Substituting Eqs. (2.3), (2.5), and (2.7) into Eq. (3.4), we obtain

$$\frac{Z_1(k)}{Z_0} = \eta_0 \sum_n \lambda_n \chi_n \left\{ \xi_n + \int_{S_1} dS\ \boldsymbol{e}_n\cdot\left[\boldsymbol{w}^+\cos\left(\frac{kg}{2}\right) - \boldsymbol{w}^-\sin\left(\frac{kg}{2}\right)\right]\right\}, \tag{3.6}$$

where we have used Eqs. (2.13), (2.20), and (2.33) to express the result in terms of $\boldsymbol{w}^+$ and $\boldsymbol{w}^-$. The constant parameter η_0 is

$$\eta_0 \equiv 2|A_0|^2/Z_0^2 C \tag{3.7}$$

and χ_n has been defined in Eq. (2.34).

Let us next transform $Z_2(k)$ into an integral form. Denoting the z component of $H_\perp$ as H_z, Eq. (3.5) together with Eq. (2.3) can be rewritten as

$$\frac{Z_2(k)}{Z_0} = \frac{\eta_0 Z_0}{2A_0}\int_{S_3} dS\ \boldsymbol{n}_h\cdot[\nabla\chi\times(H_z\boldsymbol{z})]e^{jkz}. \tag{3.8}$$

Note that $Z_2(k)$ is independent of the transverse field components and is clearly related only to TE modes. We find H_z by integrating the Maxwell equation

$$\nabla \cdot \boldsymbol{H}_\perp = -\frac{\partial H_z}{\partial z} \tag{3.9}$$

over z. Using Eq. (2.10) for $\boldsymbol{H}_\perp$, this leads to

$$\frac{Z_0 H_z}{A_0} = j \sum_\nu \frac{\lambda_\nu}{\beta_\nu} (a_\nu e^{-j\beta_\nu z} + b_\nu e^{j\beta_\nu z}) \boldsymbol{z} \cdot (\nabla \times \boldsymbol{e}_\nu). \tag{3.10}$$

Substituting this equation into Eq. (3.8) and performing the z integration, we have

$$\frac{Z_2(k)}{Z_0} = j\eta_0 \sum_\nu \frac{\lambda_\nu}{\beta_\nu} F_\nu \left\{ \frac{a_\nu}{k-\beta_\nu} \sin\left[(k-\beta_\nu)\frac{g}{2}\right] + \frac{b_\nu}{k+\beta_\nu} \sin\left[(k+\beta_\nu)\frac{g}{2}\right] \right\}, \tag{3.11}$$

where

$$F_\nu \equiv \oint_{C_h} d\ell \; \boldsymbol{n}_h \cdot (\nabla\chi \times \boldsymbol{z}) \boldsymbol{z} \cdot (\nabla \times \boldsymbol{e}_\nu), \tag{3.12}$$

which is a line integral along the iris hole boundary denoted by C_h. As shown in the Appendix, F_ν can be rewritten as

$$F_\nu = (\beta_\nu^2 - k^2)\zeta_\nu. \tag{3.13}$$

Substituting this equation into (3.11) and using Eqs. (2.17), (2.21), and (2.33), we obtain

$$\frac{Z_2(k)}{Z_0} = -j \sum_\nu^{\text{TE}} \zeta_\nu \left[\sin\frac{kg}{2} - \lambda_\nu \cos\frac{kg}{2} \tan\frac{\beta_\nu g}{2} \right] w_\nu^+ - j \sum^{\text{TE}} \zeta_\nu \left[\cos\frac{kg}{2} - \lambda_\nu \sin\frac{kg}{2} \cot\frac{\beta_\nu g}{2} \right] w_\nu^-, \tag{3.14}$$

where we have used the fact that $\zeta_\nu = 0$ for TM modes and that $\lambda_\nu = \beta_\nu/k$ for TE modes. Because $\boldsymbol{e}_\nu$ is a complete set in S_1, we can write

$$\sum_\nu \zeta_\nu w_\nu^+ = \int_{S_1} dS \; \nabla(\chi - \sigma) \cdot \boldsymbol{w}^+,$$
$$\sum_\nu \zeta_\nu w_\nu^- = \int_{S_1} dS \; \nabla(\chi - \sigma) \cdot \boldsymbol{w}^-, \tag{3.15}$$

where

$$w_\nu^+ \equiv \int_{S_1} dS \; \boldsymbol{w}^+ \cdot \boldsymbol{e}_\nu, \quad w_\nu^- \equiv \int_{S_1} dS \; \boldsymbol{w}^- \cdot \boldsymbol{e}_\nu. \tag{3.16}$$

The other terms in Eq. (3.14) can be written as

$$\int_{S_1} dS \; \nabla(\chi - \sigma) \cdot \int_{S_1} dS' \Bigg(\cos(kg/2) j \sum_\nu \lambda_\nu \boldsymbol{e}_\nu(\boldsymbol{r}) \boldsymbol{e}_\nu(\boldsymbol{r}') \times \tan(\beta_\nu g/2) \cdot \boldsymbol{w}^+(\boldsymbol{r}') + \sin(kg/2) j \sum_\nu \lambda_\nu \boldsymbol{e}_\nu(\boldsymbol{r}) \boldsymbol{e}_\nu(\boldsymbol{r}') \times \cot(\beta_\nu g/2) \cdot \boldsymbol{w}^-(\boldsymbol{r}') \Bigg). \tag{3.17}$$

Note that these terms are essentially the second terms on the left-hand side of Eqs. (2.26) and (2.27) using the two term separation of the kernels in Eqs. (2.28) and (2.29). Replacing them by the first term on the left-hand side of Eqs. (2.26) and (2.27) as well as $\boldsymbol{P}^+(\boldsymbol{r})$ and $\boldsymbol{P}^-(\boldsymbol{r})$, we finally obtain

$$\frac{Z(k)}{Z_0} = \eta_0 \left[G(k) - \frac{Z^+(k)}{Z_0} - \frac{Z^-(k)}{Z_0} \right], \tag{3.18}$$

where

$$G(k) = \sum_n^{\text{TM}} \lambda_n \xi_n^2 \tag{3.19}$$

and

$$\frac{Z^+(k)}{Z_0} = \int_{S_1} dS \; \boldsymbol{w}^+ \cdot \boldsymbol{P}^+,$$
$$\frac{Z^-(k)}{Z_0} = \int_{S_1} dS \; \boldsymbol{w}^- \cdot \boldsymbol{P}^-. \tag{3.20}$$

Finally, we note that $G(k)$ is a sum only over TM modes, since it is straightforward to show that $\xi_n = 0$ for TE modes. [See Appendix, Eq. (A19).]

IV. VARIATIONAL RESULT FOR THE IMPEDANCE

We are now in a position to write $Z^+(k)$ and $Z^-(k)$ in variational form. Specifically

$$\frac{Z^+(k)}{Z_0} = \frac{\left(\int_{S_1} dS \; \boldsymbol{w}^+ \cdot \boldsymbol{P}^+ \right)^2}{\int_{S_1} dS \int_{S_1} dS' \; \boldsymbol{w}^+(\boldsymbol{r}') \cdot \overleftrightarrow{\boldsymbol{K}}^+(\boldsymbol{r}', \boldsymbol{r}) \cdot \boldsymbol{w}^+(\boldsymbol{r})} \tag{4.1}$$

is an extremum when $\boldsymbol{w}^+$ satisfies Eq. (2.26). Thus it is possible to get an accurate value for $Z^+(k)$ by expanding $\boldsymbol{w}^+$ into a truncated complete set in S_1 and solving the resulting matrix equation. Of course an analogous expression is obtained for $Z^-(k)$.

We now use the variational form in Eq. (4.1) and a trial function for $\boldsymbol{w}^+$ of the form

$$\boldsymbol{w}^+(\boldsymbol{r}) = \sum_\nu c_\nu \boldsymbol{f}_\nu(\boldsymbol{r}), \tag{4.2}$$

where the $\boldsymbol{f}_\nu$ form a complete set (not necessarily orthogonal) in the region S_1. If we truncate the sum in Eq. (4.2) and minimize Eq. (4.1) by varying c_ν, it is straightforward to show that the result is equivalent to substituting Eq. (4.2) into Eq. (2.26), multiplying by $\boldsymbol{f}_\nu(\boldsymbol{r})$, and integrating over S_1 to obtain

$$\sum_\mu M_{\nu\mu} c_\mu = P_\nu^+, \tag{4.3}$$

where

$$P_\nu^+ \equiv \int_{S_1} dS \; \boldsymbol{P}^+ \cdot \boldsymbol{f}_\nu, \tag{4.4}$$

$$M_{\nu\mu} \equiv \int_{S_1} dS \int_{S_1} dS' \, \boldsymbol{f}_\nu(\boldsymbol{r}') \cdot \overleftrightarrow{\mathbf{K}}^+(\boldsymbol{r}', \boldsymbol{r}) \cdot \boldsymbol{f}_\mu(\boldsymbol{r}) = M_{\mu\nu}. \tag{4.5}$$

Equation (4.3) is a matrix equation whose solution is

$$c_\nu = \sum_\mu (\boldsymbol{M}^{-1})_{\nu\mu} P_\mu^+, \tag{4.6}$$

from which one obtains directly

$$\frac{Z^+}{Z_0} = \sum_\mu \sum_\nu P_\mu^+ (\boldsymbol{M}^{-1})_{\mu\nu} P_\nu^+. \tag{4.7}$$

The calculation of Z^-/Z_0 proceeds in an analogous manner with $\overleftrightarrow{\mathbf{K}}^+$ being replaced by $\overleftrightarrow{\mathbf{K}}^-$ and P_ν^+ in Eq. (4.4) being replaced by

$$P_\nu^- \equiv \int_{S_1} dS \; \boldsymbol{P}^- \cdot \boldsymbol{f}_\nu. \tag{4.8}$$

The significance of the variational form is that the result for the impedance will be quite accurate since the error will be proportional to the square of the error in $\boldsymbol{w}^+$. The error in $\boldsymbol{w}^+$ comes only from the truncation in Eq. (4.2), so the accuracy of Eq. (4.7) can be easily tested by comparing the results of different size truncations. In this way we will be able to obtain numerical results good to three or four significant figures with only modest size matrices. This will be described in detail in Sec. VIII in the numerical calculations.

Finally we note that the accuracy which is obtained from a given number of terms in Eq. (4.2) will depend on the particular complete set $\boldsymbol{f}_\nu$ which is used. Past experience [4] suggests that a form which has the correct singular dependence at the iris corner has some advantage. But in the present work it proves to be more than sufficient to use $\boldsymbol{e}_\nu$, the complete set of TM, TE modes in the iris pipe.

V. ZERO-THICKNESS LIMIT

In the zero-thickness limit, i.e., $g \to 0$, we can set $\boldsymbol{w}^- = 0$ because $\boldsymbol{u} = \boldsymbol{v}$. In addition, the contribution of the iris hole to the impedance vanishes as do the second terms in the right-hand side of Eqs. (2.28) and (2.30). In this case, defining the new integral kernel as

$$\overleftrightarrow{\boldsymbol{K}}(\boldsymbol{r}', \boldsymbol{r}) \equiv \sum_n \lambda_n \boldsymbol{e}_n(\boldsymbol{r}') \boldsymbol{e}_n(\boldsymbol{r}), \tag{5.1}$$

the variational part of the impedance can be given by

$$\frac{Z^+(k)}{Z_0} = \frac{\left(\sum_n^{\mathrm{TM}} \lambda_n \xi_n \int_{S_1} dS \; \boldsymbol{e}_n(\boldsymbol{r}) \cdot \boldsymbol{w}(\boldsymbol{r}) \right)^2}{\int_{S_1} dS \int_{S_1} dS' \; \boldsymbol{w}(\boldsymbol{r}') \cdot \overleftrightarrow{\boldsymbol{K}}(\boldsymbol{r}', \boldsymbol{r}) \cdot \boldsymbol{w}(\boldsymbol{r})}, \tag{5.2}$$

$$\frac{Z^-(k)}{Z_0} = 0,$$

where we have set $\boldsymbol{w}^+ = \boldsymbol{w}$. The explicit term defined in Eq. (3.19) remains unchanged. Note that the numerator in Eq. (5.2) depends only on TM modes because of Eq. (A19) while the denominator contains both TM and TE modes. The final result for $Z^+(k)/Z_0$ differs from that in Eq. (4.7) only in the replacement of $\overleftrightarrow{\mathbf{K}}^+$ by $\overleftrightarrow{\mathbf{K}}$ in Eq. (4.5).

VI. CIRCULAR IRIS IN A CYLINDRICAL BEAM PIPE—LONGITUDINAL IMPEDANCE

We now particularize the previous analysis to a circular iris of radius b in a cylindrical beam pipe of radius a and obtain explicit expressions for the quantities which enter the calculation of the longitudinal coupling impedance. We start with Eq. (2.3) and set

$$\chi(r) = \sigma(r) = -\ln r \; , \; A_0 = Z_0 I_0 / 2\pi. \tag{6.1}$$

The constant η_0 in Eq. (3.7) has the value $1/2\pi^2$.

TE modes do not contribute to the longitudinal impedance. The solutions of Eqs. (A1)–(A4) for the normalized TM modes are

$$\phi_n = \frac{J_0(s_n r/a)}{\sqrt{\pi} s_n J_1(s_n)} \; , \; \phi_\nu = \frac{J_0(s_\nu r/b)}{\sqrt{\pi} s_\nu J_1(s_\nu)}, \tag{6.2}$$

where $J_n(z)$ denotes the Bessel function of nth order, $s_{n(\nu)}$ is the nth (νth) zero of $J_0(s) = 0$, and the mode $\boldsymbol{e}_{n(\nu)}$ is obtained from Eqs. (A5) and (A6). The propagation constants are given by

$$\beta_n = (k^2 - s_n^2/a^2)^{1/2} = -j(s_n^2/a^2 - k^2)^{1/2}, \tag{6.3}$$

$$\beta_\nu = (k^2 - s_\nu^2/b^2)^{1/2} = -j(s_\nu^2/b^2 - k^2)^{1/2}. \tag{6.4}$$

Using Eqs. (6.1) and (A5), we have from Eq. (2.14)

$$\xi_n = \frac{2\sqrt{\pi} J_0(s_n b/a)}{s_n J_1(s_n)}. \tag{6.5}$$

Noting that $\lambda_n = k/\beta_n$ for TM modes, substitution of Eq. (6.5) into Eq. (3.19) leads to

$$G_\parallel(k) = 4\pi \sum_n \frac{k}{\beta_n} \left[\frac{J_0(s_n b/a)}{s_n J_1(s_n)} \right]^2. \tag{6.6}$$

Dropping the TE terms in Eqs. (2.30) and (2.31), we have

$$\boldsymbol{P}^+ = -\cos\frac{kg}{2} \sum_n \frac{k}{\beta_n} \xi_n \boldsymbol{e}_n,$$

$$\boldsymbol{P}^- = \sin\frac{kg}{2} \sum_n \frac{k}{\beta_n} \xi_n \boldsymbol{e}_n. \tag{6.7}$$

We now use the complete set $\boldsymbol{e}_\nu$ as the expansion basis in Eq. (4.2). This leads to

$$P_\nu^+ = -\cos\frac{kg}{2} \sum_n \frac{k}{\beta_n} \xi_n K_{n\nu}^L,$$

$$P_\nu^- = \sin\frac{kg}{2} \sum_n \frac{k}{\beta_n} \xi_n K_{n\nu}^L, \tag{6.8}$$

where

$$K^L_{n\nu} \equiv \int_{S_1} dS\, \boldsymbol{e}_n \cdot \boldsymbol{e}_\nu \text{ (longitudinal impedance).} \quad (6.9)$$

For TM modes

$$K^L_{n\nu} = \frac{2b^2 s_n J_0(s_n b/a)}{a^2 J_1(s_n)[s_\nu^2 - (s_n b/a)^2]}. \quad (6.10)$$

The matrix elements $M_{\mu\nu}$ can similarly be obtained. Specifically, using Eqs. (2.28) and (4.5), with $\boldsymbol{f}_\nu = \boldsymbol{e}_\nu$, we find

$$M_{\mu\nu} = \sum_n \frac{k}{\beta_n} K^L_{n\mu} K^L_{n\nu} + \frac{jk}{\beta_\nu} \tan\left(\frac{\beta_\nu g}{2}\right) \delta_{\mu\nu} \quad (6.11)$$

with $\tan(\beta_\nu g/2)$ being replaced by $-\cot(\beta_\nu g/2)$ in the calculation of $Z^-(k)$. Finally, we fold Eqs. (6.8), (6.10), and (6.11) into Eq. (4.7) to obtain an explicit expression for Z^+/Z_0 and the corresponding expression for Z^-/Z_0.

VII. CIRCULAR IRIS IN A CYLINDRICAL BEAM PIPE—TRANSVERSE IMPEDANCE

For the transverse impedance we again start with Eq. (2.3) and set

$$\chi(r,\theta) = \left(\frac{r}{a^2} - \frac{1}{r}\right)\cos\theta,$$
$$\sigma(r,\theta) = \left(\frac{r}{b^2} - \frac{1}{r}\right)\cos\theta, \quad (7.1)$$

$$A_0 = Z_0 I_0 \Delta/\pi. \quad (7.2)$$

In this case, using Eq. (3.7), the constant η_0 has the value

$$\eta_0 = \frac{2|A_0|^2}{4k\Delta^2 Z_0^2 |I_0|^2} = \frac{1}{2\pi^2 k}. \quad (7.3)$$

Denoting the nth (νth) zeros of $J_1(s)$ and dJ_1/ds as $p_{n(\nu)}$ and $q_{n(\nu)}$, respectively, we can write the scalar mode functions in the pipe region as

$$\phi_n = \sqrt{\frac{2}{\pi}} \frac{1}{p_n J_0(p_n)} J_1\left(p_n \frac{r}{a}\right)\cos\theta \quad \text{for TM modes,} \quad (7.4)$$

$$\psi_n = \sqrt{\frac{2}{\pi}} \frac{1}{\sqrt{q_n^2 - 1}\, J_1(q_n)} J_1\left(q_n \frac{r}{a}\right)\sin\theta \quad \text{for TE modes,} \quad (7.5)$$

and in the iris region as

$$\phi_\nu = \sqrt{\frac{2}{\pi}} \frac{1}{p_\nu J_0(p_\nu)} J_1\left(p_\nu \frac{r}{b}\right)\cos\theta \text{ for TM modes,} \quad (7.6)$$

$$\psi_\nu = \sqrt{\frac{2}{\pi}} \frac{1}{\sqrt{q_\nu^2 - 1}\, J_1(q_\nu)} J_1\left(q_\nu \frac{r}{b}\right)\sin\theta \quad \text{for TE modes.} \quad (7.7)$$

Substituting Eqs. (A5) and (A6) together with Eqs. (7.4)–(7.7) into Eqs. (2.14) and (2.32), we have

$$\xi_n = \begin{cases} \sqrt{8\pi} J_1(p_n b/a)/b p_n J_0(p_n) & \text{for TM modes} \\ 0 & \text{for TE modes,} \end{cases} \quad (7.8)$$

$$\zeta_\nu = \begin{cases} 0 & \text{for TM modes} \\ \sqrt{2\pi}(a^2 - b^2)(q_\nu^2 - 1)^{-1/2}/ba^2 & \text{for TE modes.} \end{cases} \quad (7.9)$$

From Eqs. (3.19) and (7.8) we obtain for the explicit term

$$G_\perp(k) = \frac{8\pi}{b^2} \sum_n \frac{k}{\beta_n} \left[\frac{J_1(p_n b/a)}{p_n J_0(p_n)}\right]^2. \quad (7.10)$$

We now have

$$P_\nu^+ = -\cos\left(\frac{kg}{2}\right) \sum_n^{\text{TM}} \frac{k}{\beta_n} \xi_n K^T_{n\nu} + j \sin\left(\frac{kg}{2}\right) \zeta_\nu, \quad (7.11)$$

$$P_\nu^- = \sin\left(\frac{kg}{2}\right) \sum_n^{\text{TM}} \frac{k}{\beta_n} \xi_n K^T_{n\nu} + j \cos\left(\frac{kg}{2}\right) \zeta_\nu, \quad (7.12)$$

where

$$K^T_{n\nu} \equiv \int_{S_1} dS\, \boldsymbol{e}_n \cdot \boldsymbol{e}_\nu \text{ (transverse impedance).} \quad (7.13)$$

In addition, for $\boldsymbol{f}_\nu = \boldsymbol{e}_\nu$ we have

$$M_{\mu\nu} = \sum_n \lambda_n K^T_{n\mu} K^T_{n\nu} + j\lambda_\nu \tan\left(\frac{\beta_\nu g}{2}\right) \delta_{\mu\nu} \quad (7.14)$$

in the result for Z^+, where n, μ, ν now include both TM and TE modes. For Z^-, the matrix elements are obtained as before by replacing $\tan(\beta_\nu g/2)$ by $-\cot(\beta_\nu g/2)$. Finally we fold Eqs. (7.11)–(7.14) into Eq. (4.7) to obtain an explicit expression for Z^+/Z_0 and the corresponding expression for Z^-/Z_0.

To complete this section, we give explicit expressions for $K^T_{n\nu}$ for TM and TE modes. Specifically

1. n: TM, ν: TM

$$K^T_{n\nu} = -\frac{2b^2 p_n J_1(p_n b/a)}{a^2 J_0(p_n)[p_\nu^2 - (p_n b/a)^2]}, \quad (7.15)$$

2. n: TM, ν: TE

$$K^T_{n\nu} = \frac{2J_1(p_n b/a)}{\sqrt{q_\nu^2 - 1}\, p_n J_0(p_n)}, \quad (7.16)$$

3. n: TE, ν: TM

$$K^T_{n\nu} = 0, \quad (7.17)$$

4. n: TE, ν: TE

$$K^T_{n\nu} = \frac{2bq_\nu^2 q_n J_1'(q_n b/a)}{a\sqrt{q_n^2 - 1}\sqrt{q_\nu^2 - 1} J_1(q_n)[q_\nu^2 - (q_n b/a)^2]}, \quad (7.18)$$

where $J_1'(s) \equiv dJ_1(s)/ds$.

VIII. NUMERICAL RESULTS

The results in Sec. VI are the same as those obtained earlier [5] for the longitudinal impedance. In that work our emphasis was on large values of a/b (10,25,100,1000) and a range of values of g/b from 0 to 5 in order to understand the impedance of a hole in a thick plate. As will be discussed in Sec. IX, we found that the sum in Eq. (6.6) diverged if we proceeded to the limit $b/a = 0, \beta_n = k$ and eventually extracted $(1/\pi)\ln(a/b)$ from Eq. (3.18) to obtain finite results for large a/b. The results are reproduced in Figs. 1–4 for

$$\frac{Z(k)}{Z_0} \equiv R + jX, \tag{8.1}$$

where

$$R \equiv \frac{1}{\pi}\ln\frac{a}{b} + R' \equiv \frac{1}{\pi}\ln ka + R''. \tag{8.2}$$

The results in Sec. VII for the transverse impedance are also related to earlier work [6], but in that work we did not use a variational form for the impedance. As a result the calculations converged quite slowly, requiring the use of very large matrices which were often quite singular. Nevertheless in that case we obtained results which were finite in the limit of large a/b.

We have now used the variational calculation outlined in Sec. VII and obtain well convergent results which are consistent with the earlier work [6]. But the calculations

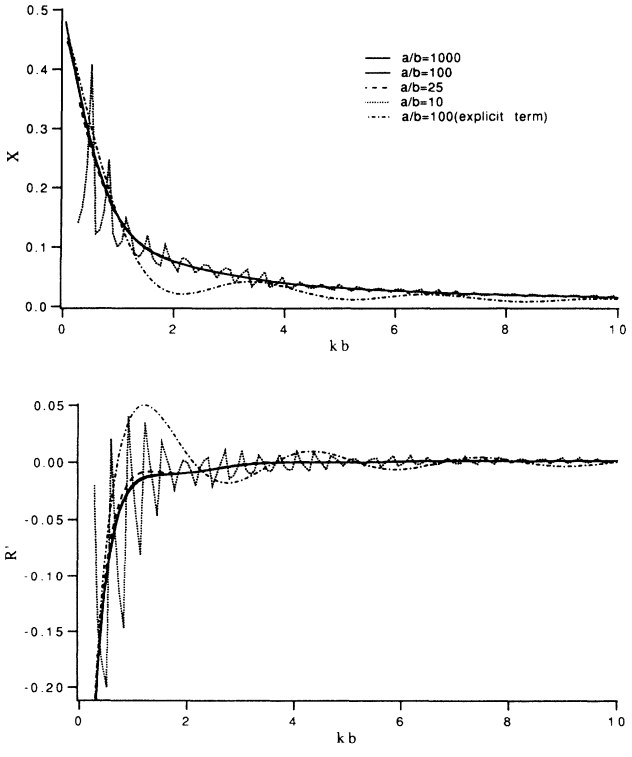

FIG. 1. Real and imaginary parts of the longitudinal impedance as a function of kb for $g/b = 0$ and $a/b = 10$, 25, 100, and 1000. Also included is the explicit term defined in Eq. (11.1) for $a/b = 100$.

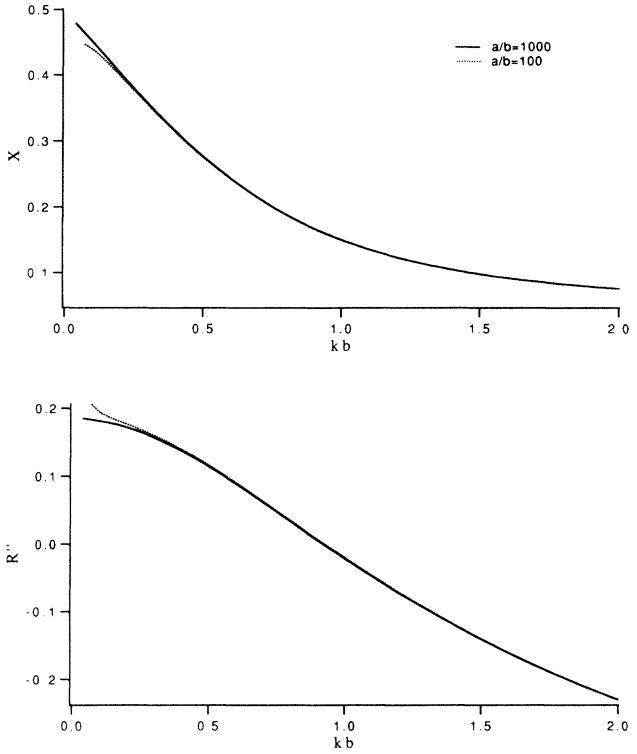

FIG. 2. Real and imaginary parts of the longitudinal impedance as a function of kb for $g/b = 0$ and $a/b = 100$ and 1000.

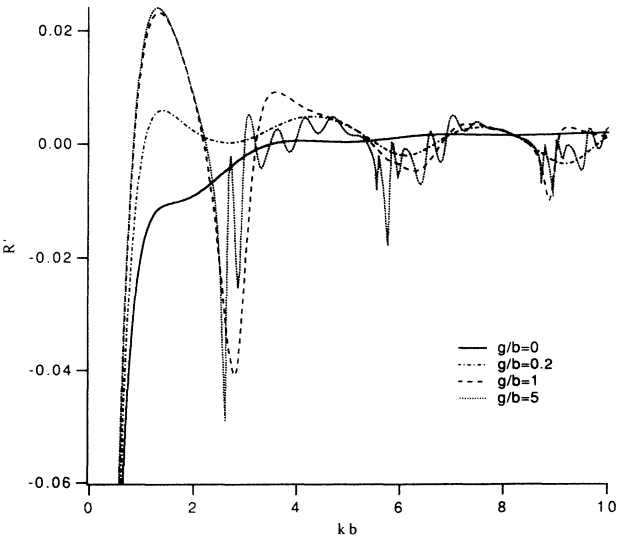

FIG. 3. Real and imaginary parts of the longitudinal impedance as a function of kb for $a/b = 100$ and $g/b = 0$, 0.2, 1, and 5.

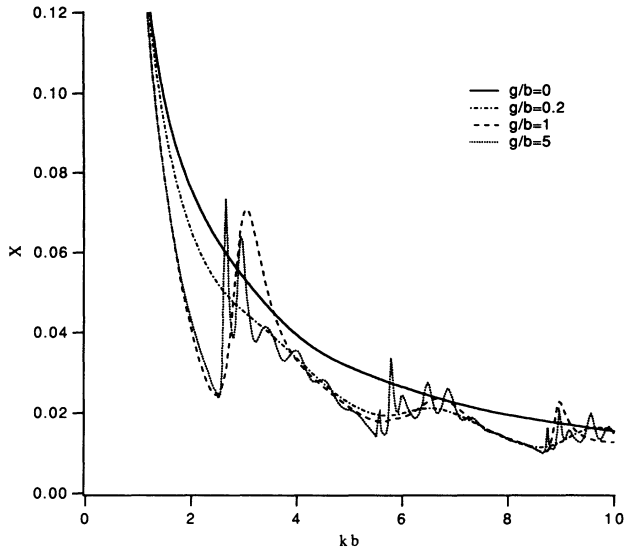

FIG. 4. Imaginary parts of the longitudinal impedance as a function of kb for $a/b = 100$ and $g/b = 0$, 0.2, 1, and 5.

are much simpler and more accurate. Figure 5 shows the result for $a/b = 100$, and $g/b = 1$ as a function of kb for different size matrices and it is clear the result does not change significantly for matrix sizes greater than 2×2 (one TM mode and one TE mode in the iris region). Figure 6 shows the result as a function of the number

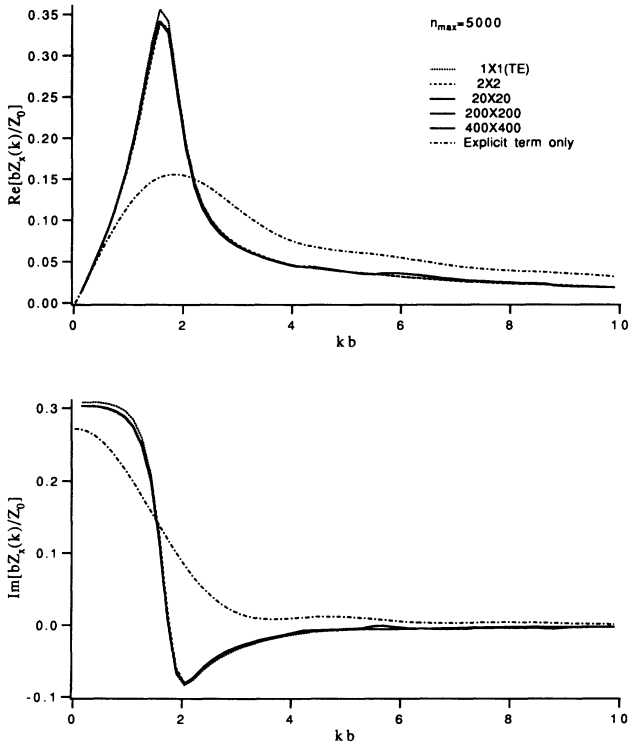

FIG. 5. Real and imaginary parts of the transverse impedance as a function of kb for $a/b = 100$ and $g/b = 1$ using $n_{\max} = 500$ with matrix sizes 1(TE), 2, 20, 200, and 400. Also included is the explicit term defined in Eq. (11.2) for $a/b = 100$.

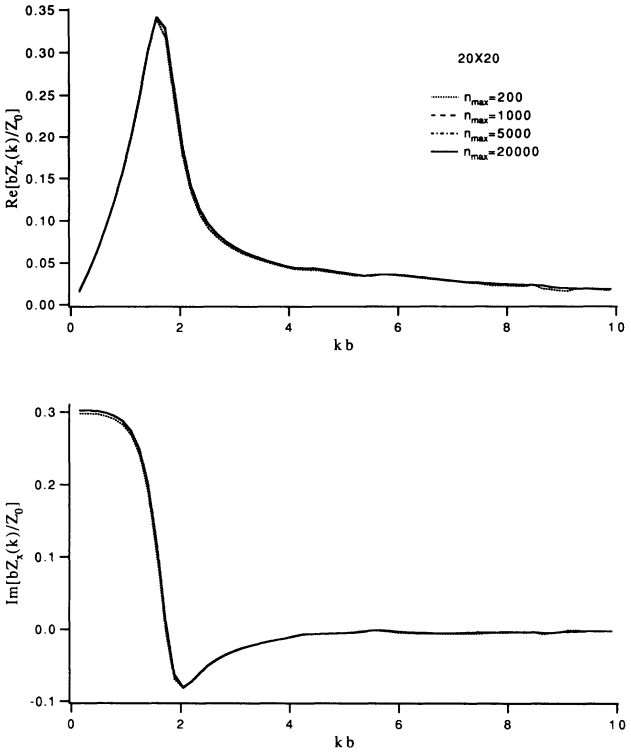

FIG. 6. Real and imaginary parts of the transverse impedance as a function of kb for $a/b = 100$ and $g/b = 1$ using matrix size 20 with $n_{\max} = 1000$, 5000, and 20 000.

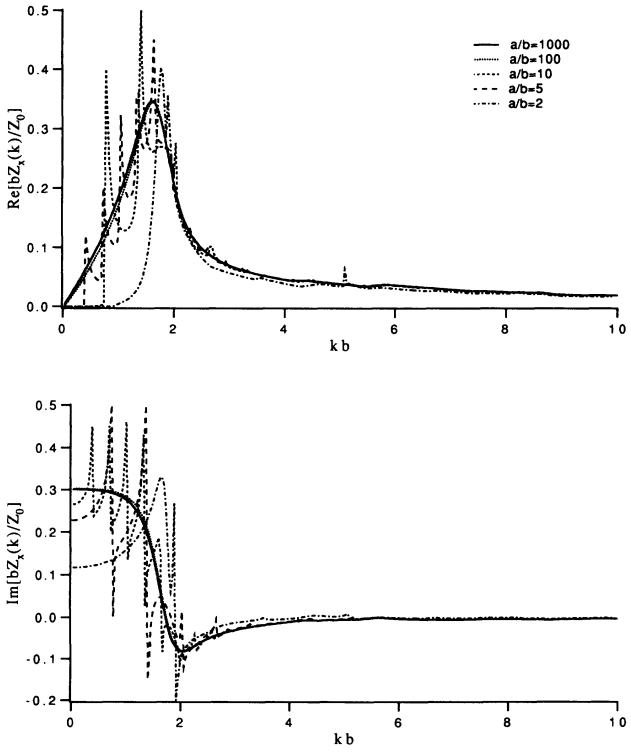

FIG. 7. Real and imaginary parts of the transverse impedance as a function of kb for $g/b = 1$ and $a/b = 2$, 5, 10, 100, and 1000.

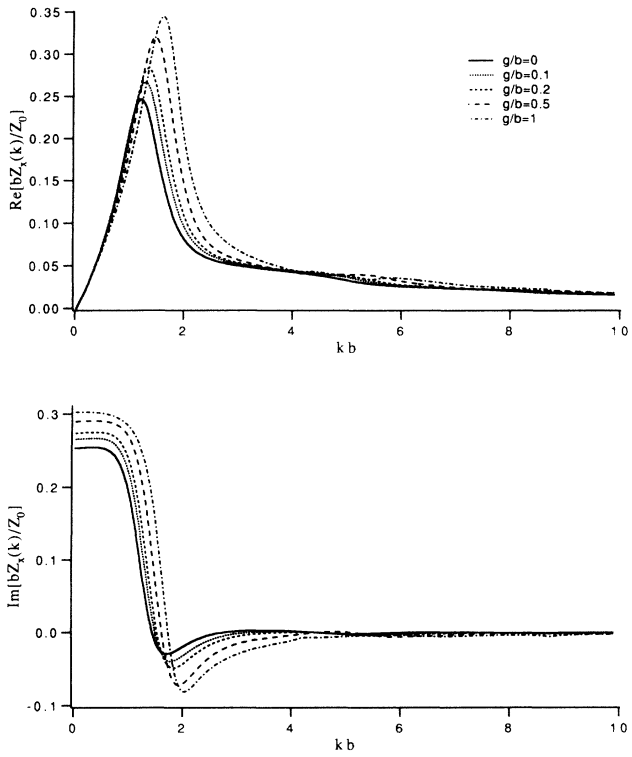

FIG. 8. Real and imaginary parts of the transverse impedance as a function of kb for $a/b = 100$ and $g/b = 0$, 0.1, 0.2, 0.5, and 1.

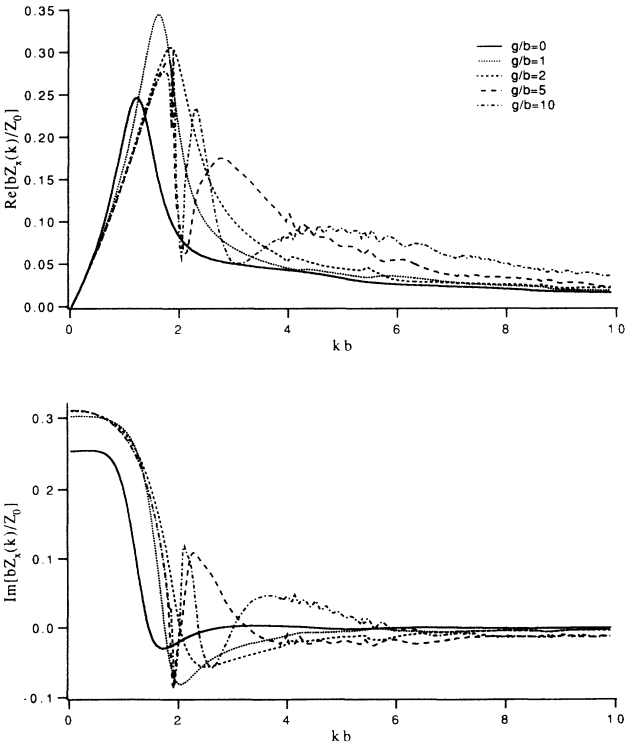

FIG. 9. Real and imaginary parts of the transverse impedance as a function of kb for $a/b = 100$ and $g/b = 0$, 1, 2, 5, and 10.

of terms in the sums over n in Eqs. (7.10)–(7.14). No noticeable change occurs for $n_{\max} > 1000$. To be on the safe side, we use 20×20 matrices with $n_{\max} = 5000$. Figure 7 shows the impedance for $g/b = 1$ and $a/b = 2$, 5, 10, 100, and 1000. In this figure we have performed an average over rapid oscillations for $a/b \geq 100$. Except for high frequency details, the results are remarkably insensitive to a/b. The impedance is shown in Figs. 8 and 9 for $a/b = 100$ for values of g/b ranging from 0 to 10.

The results indicate a general pattern which is remarkably independent of the values of both a/b and g/b. Specifically, the real part of the impedance (in units of Z_0/b) starts with 0 at $kb = 0$, reaches a peak of order 0.3 near $kb = 2$, and thereafter falls off roughly as $1/kb$. Similarly, the imaginary part starts with a finite value of 0.2–0.3 at $kb = 0$ decreases through zero to a negative value at about $kb = 2$ and then rapidly approaches 0 roughly as $(kb)^{-3/2}$. In Sec. X we shall examine these limits in greater detail.

IX. IMPEDANCE OF A HOLE: LIMIT FOR INFINITE BEAM PIPE RADIUS

In Sec. III we derived a general form for the impedance in Eq. (3.18). For the longitudinal impedance of a circular iris this takes the specific form

$$\frac{Z_{\parallel}(k)}{Z_0} = \frac{1}{2\pi^2}\left[G_{\parallel}(k) - \frac{Z_{\parallel}^{+}(k)}{Z_0} - \frac{Z_{\parallel}^{-}(k)}{Z_0}\right], \tag{9.1}$$

where $G_{\parallel}(k)$ is given in Eq. (6.6). The impedance $Z_{\parallel}^{+}(k)$ [and by implication $Z_{\parallel}^{-}(k)$] is obtained from Eq. (4.7):

$$\frac{Z_{\parallel}^{\pm}}{Z_0} = \sum_{\mu}\sum_{\nu} P_{\mu}^{\pm}(M^{-1})_{\mu\nu}P_{\nu}^{\pm}, \tag{9.2}$$

where $P_{\nu}^{\pm}$ is given in Eqs. (6.8) and (6.10) and the matrix elements $M_{\mu\nu}$ are given in Eq. (6.11).

As $b/a \to 0$, it is clear that the contributions to the sums over n in Eqs. (6.6), (6.8), and (6.11) come primarily from terms with large n. Moreover the sum over n can now be converted to an integral over α by the replacements

$$\frac{s_n b}{a} \to \alpha\ , \quad \sum_{n=1}^{\infty} \to \frac{a}{\pi b}\int_0^{\infty} d\alpha, \tag{9.3}$$

where the spacing of the roots s_n is taken to be π for large n. We also replace $b\beta_n$ by

$$b\beta_n = \sqrt{k^2b^2 - (s_n b/a)^2} \to \sqrt{k^2b^2 - \alpha^2} \tag{9.4}$$

and use the large s_n approximation

$$J_1^2(s_n) \cong \frac{2}{\pi s_n} \to \frac{2b}{\pi a \alpha}. \tag{9.5}$$

In this way we obtain

$$G_{\|}(k) = 4\pi \sum_n \frac{J_0^2(s_n b/a)}{s_n^2 J_1^2(s_n)} + 2\pi \int_0^\infty \frac{d\alpha}{\alpha} J_0^2(\alpha) \left[\frac{kb}{\sqrt{k^2b^2 - \alpha^2}} - 1 \right], \quad (9.6)$$

where we have separated $G_{\|}(k)$ into one term containing a logarithmic divergence as $a/b \to \infty$ and another which is convergent in that limit [5]. The first term can be evaluated by expanding the function

$$f(r) = \begin{cases} \ln(a/b) \ , & 0 \le r \le b \\ \ln(a/r) \ , & b \le r \le a \end{cases} \quad (9.7)$$

into the complete set $J_0(s_n r/a)$, leading to

$$G_{\|}(k) = 2\pi \ln \frac{a}{b} + 2\pi \int_0^\infty \frac{d\alpha}{\alpha} J_0^2(\alpha) \left[\frac{kb}{\sqrt{k^2b^2 - \alpha^2}} - 1 \right]. \quad (9.8)$$

We also find

$$P_\nu^+ = -2\sqrt{\pi} \cos(kg/2) \ S_\nu,$$
$$P_\nu^- = 2\sqrt{\pi} \sin(kg/2) \ S_\nu, \quad (9.9)$$

where

$$S_\nu \equiv \int_0^\infty \frac{\alpha d\alpha \ kbJ_0^2(\alpha)}{\sqrt{k^2b^2 - \alpha^2}(s_\nu^2 - \alpha^2)} \quad (9.10)$$

and

$$M_{\mu\nu}^{\pm} = \frac{jk}{\beta_\nu} \tan \frac{\beta_\nu g}{2} \delta_{\mu\nu} + 2 \left(\frac{s_\mu^2 P_\mu^{\pm} - s_\nu^2 P_\nu^{\pm}}{s_\nu^2 - s_\mu^2} \right). \quad (9.11)$$

These forms permit one to obtain results directly for $a/b \to \infty$ rather than performing the calculations for several large values of a/b, also avoiding the averaging process needed for large a/b. But consistent results have already been obtained for large a/b and we have not found it necessary to implement the process outlined in this section.

The large a/b limit for the transverse impedance can be obtained in an analogous manner. We now have

$$\frac{bZ_\perp(k)}{Z_0} = \frac{b}{2\pi^2 k} \left[G_\perp(k) - \frac{Z_\perp^+(k)}{Z_0} - \frac{Z_\perp^-(k)}{Z_0} \right], \quad (9.12)$$

where we have included a factor b to make Eq. (9.12) dimensionless. Replacing $p_n b/a$ by α as before, we find the convergent result

$$b^2 G_\perp(k) = 4\pi \int_0^\infty \frac{d\alpha}{\alpha} \frac{kbJ_1^2(\alpha)}{\sqrt{k^2b^2 - \alpha^2}}. \quad (9.13)$$

The limiting forms for $P_\nu^{\pm}$ and $M_{\mu\nu}^{\pm}$ for the transverse impedance are similar to those in Eqs. (9.9)–(9.11), but they are not given here because they are somewhat more complicated since n and ν refer to both TM and TE modes for which the expressions differ.

Finally, we give simple expressions for the real parts of $G_{\|}(k)$ and $G_\perp(k)$ obtained from Eqs (9.8) and (9.13) by using integral representations for $J_0^2(\lambda)$ and $J_1^2(\lambda)$. They are

$$\mathrm{Re}G_{\|}(k) = 2\pi \ell n \frac{a}{b} - 2\pi \int_{kb}^\infty \frac{d\lambda}{\lambda} J_0(2\lambda), \quad (9.14)$$

$$\mathrm{Re}G_\perp(k) = 2\pi \left(1 - \frac{J_1(2kb)}{kb} \right). \quad (9.15)$$

Efforts to obtain similarly simple expressions for the imaginary parts have not been successful.

X. WAKE FUNCTION, CAUSALITY, AND SUM RULES

In Eq. (1.3) of Sec. I we defined the longitudinal impedance $Z_{\|}(k)$ in terms of the electric field in the frequency domain. Another quantity which is of frequent interest is the longitudinal wake function which we define as

$$W_{\|}(\zeta) = \frac{1}{cQ} \int_{-\infty}^\infty dz \ E_z \left(0, 0, z; \frac{z+\zeta}{c} \right), \quad (10.1)$$

representing some sort of average a distance ζ behind the test charge. As it turns out [1], this implies the transform pair

$$W_{\|}(\zeta) = \frac{1}{2\pi} \int_{-\infty}^\infty dk \ e^{jk\zeta} Z_{\|}(k) \quad (10.2)$$

and

$$Z_{\|}(k) = \int_0^\infty d\zeta \ W_{\|}(\zeta) \ e^{-jk\zeta}, \quad (10.3)$$

where the integral in Eq. (10.3) extends only over positive values of ζ since the wake function ahead of source charge must vanish in the limit $\gamma \to \infty$ because of causality.

Since we expect $W_{\|}(\zeta)$ to be finite and to vanish as $\zeta \to \infty$, Eq. (10.3) tells us that $Z_{\|}(k)$ must be analytic in the lower half k plane. In addition, $W_{\|}(\zeta)$ as defined in Eq. (10.1) is real, so that we must have

$$Z_{\|}(-k) = Z_{\|}^*(k) \quad (10.4)$$

or

$$R_{\|}'(-k) = R_{\|}'(k) \ , \ X_{\|}(-k) = -X_{\|}(k), \quad (10.5)$$

where $Z_{\|}'(k)/Z_0 \equiv R_{\|}'(k) + jX_{\|}(k)$ and we have removed the constant term $(1/\pi)\ln(a/b)$ from $R_{\|}(k)$, as defined in Eq. (8.2). These equations yield a real wake function in Eq. (10.2). Therefore

$$W_{\|}(\zeta)/Z_0 = \frac{1}{\pi} \int_0^\infty dk [R_{\|}'(k) \cos k\zeta - X_{\|}(k) \sin k\zeta], \quad (10.6)$$

where the constant term in $R_{\|}(k)$ makes no contribution. And the requirement that $W_{\|}(\zeta) = 0$ for $\zeta < 0$ allows us to write

$$W_{\|}(\zeta)/Z_0 = \frac{2}{\pi} \int_0^\infty dk \ R_{\|}'(k) \cos k\zeta = -\frac{2}{\pi} \int_0^\infty dk \ X_{\|}(k) \sin k\zeta, \quad (10.7)$$

enabling us to obtain the wake function from either the real or the imaginary part of the impedance.

The analytic behavior of $Z_\parallel(k)$ in the lower half k plane allows us to invoke the Kramers-Kronig relations

$$R'_\parallel(k) = -\frac{2}{\pi}\mathrm{P}\int_0^\infty dk' \frac{k' X_\parallel(k')}{k'^2 - k^2}, \tag{10.8}$$

$$X_\parallel(k) = \frac{2k}{\pi}\mathrm{P}\int_0^\infty dk' \frac{R'_\parallel(k')}{k'^2 - k^2}, \tag{10.9}$$

where P stands for the principal value of the integral which follows.

Similar results are available for the transverse wake function and impedance. In this case, however, there is an extra factor k^{-1} in the definition of the transverse impedance and we therefore have [7]

$$W_\perp(\zeta) = \frac{1}{2\pi}\int_{-\infty}^\infty dk\ k\ Z_\perp(k) e^{jk\zeta} \tag{10.10}$$

and

$$kZ_\perp(k) = \int_0^\infty d\zeta\ W_\perp(\zeta) e^{-jk\zeta}. \tag{10.11}$$

The transverse impedance is again analytic in the lower half k plane, but this time we must have

$$Z_\perp(-k) = -Z_\perp^*(k) \tag{10.12}$$

or

$$R_\perp(-k) = -R_\perp(k)\ ,\ X_\perp(-k) = X_\perp(k), \tag{10.13}$$

where $Z_\perp(k)/Z_0 \equiv R_\perp(k) + jX_\perp(k)$. This leads to

$$\begin{aligned} W_\perp(\zeta)/Z_0 &= \frac{2}{\pi}\int_0^\infty k\ dk\ R_\perp(k)\cos k\zeta \\ &= -\frac{2}{\pi}\int_0^\infty k\ dk\ X_\perp(k)\sin k\zeta \end{aligned} \tag{10.14}$$

and

$$R_\perp(k) = -\frac{2k}{\pi}\mathrm{P}\int_0^\infty dk' \frac{X_\perp(k')}{k'^2 - k^2}, \tag{10.15}$$

$$X_\perp(k) = \frac{2}{\pi}\mathrm{P}\int_0^\infty dk' \frac{k' R_\perp(k')}{k'^2 - k^2}. \tag{10.16}$$

From Eqs. (10.15) and (10.16) we can readily determine the behavior of $R_\perp(k)$ and $X_\perp(k)$ as $k \to 0$. Specifically

$$R_\perp(0) = 0\ ,\ X_\perp(0) = \frac{2}{\pi}\int_0^\infty R(k')\frac{dk'}{k'}, \tag{10.17}$$

$$\lim_{k\to 0}[R_\perp(k)/k] = \int_0^\infty dk' \frac{[X_\perp(k') - X(0)]}{k'^2}. \tag{10.18}$$

For large k, Eq. (10.15) reduces to

$$R_\perp(k) \to \frac{2}{\pi k}\int_0^\infty dk' X(k'). \tag{10.19}$$

Since the integral on the right-hand side converges, we see that $R_\perp(k)$ is proportional to k^{-1} as $k \to \infty$. At the same time, the large k behavior of Eq. (10.16) requires more careful consideration. In particular, we try

$$bR_\perp(k) \to A(kb)^{-1} + B(kb)^{-3/2}, \tag{10.20}$$

where A and B are dimensionless numbers. Since

$$\mathrm{P}\int_0^\infty \frac{dk'}{k'^2 - k^2} = \frac{1}{2k}\ln\frac{|k' - k|}{k' + k}\bigg|_0^\infty = 0, \tag{10.21}$$

we have

$$X_\perp(k) \to \frac{Bb^{-3/2}}{\pi k}\mathrm{P}\int_0^\infty \frac{dk'}{\sqrt{k'}}\left(\frac{1}{k' - k} - \frac{1}{k' + k}\right). \tag{10.22}$$

Setting $k' = u^2$, we find

$$\begin{aligned} X_\perp(k) &\to \frac{2Bb^{-3/2}}{\pi k}\mathrm{P}\int_0^\infty du\left[\frac{1}{u^2 - k} - \frac{1}{u^2 + k}\right] \\ &= -\frac{B}{(kb)^{3/2}}. \end{aligned} \tag{10.23}$$

Thus we have

$$\frac{bZ_\perp(k)}{Z_0} \to \frac{A}{kb} + \frac{(1-j)B}{(kb)^{3/2}}. \tag{10.24}$$

Close examination of the behavior of $R_\perp(k)$ and $X_\perp(k)$ confirms the validity of Eq. (10.24) for large k.

In a similar way we can examine the behavior of $R'_\parallel(k)$

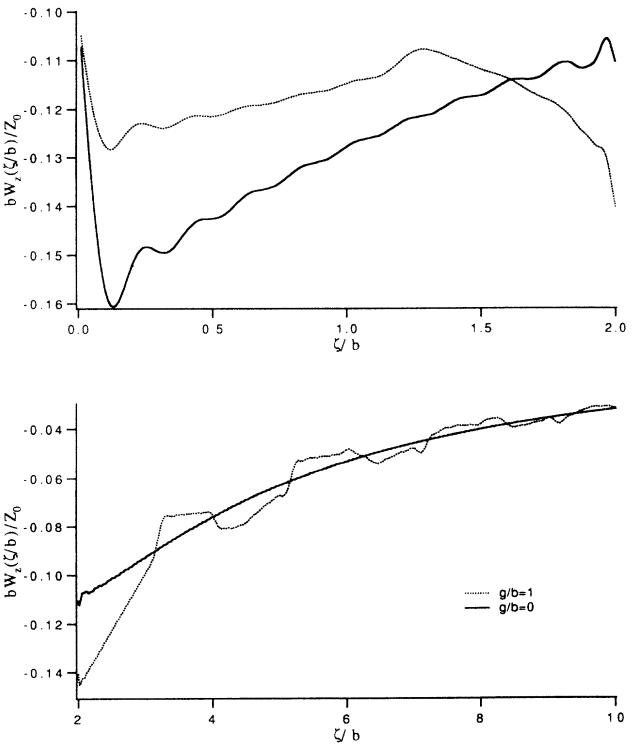

FIG. 10. Longitudinal wake function in units of Z_0/b for $a/b = 100$ and $g/b = 0$ and 1.

and $X_\parallel(k)$ as $k \to \infty$. Specifically we find

$$R'_\parallel(k) \to \frac{2}{\pi k^2}\int_0^\infty dk' \left[\lim_{k'\to\infty} k' X_\perp(k') - k' X_\parallel(k')\right], \tag{10.25}$$

$$X_\parallel(k) \to \frac{2}{\pi k}\int_0^\infty dk' R'_\parallel(k'), \tag{10.26}$$

where the additional term in Eq. (10.25) makes the result for $R'_\parallel(k)$ finite.

Finally we examine the behavior of the wake functions for small ζ, a region important for short bunches. Using the second form in Eq. (10.7) and recognizing that the behavior at small ζ depends on the behavior at large k, we obtain from Eq. (10.7)

$$W_\parallel(0)/Z_0 = \frac{2}{\pi}\int_0^\infty dk R'_\parallel(k), \tag{10.27}$$

a result which is consistent with the first form in Eq. (10.7) with $\zeta = 0$.

For the transverse impedance the asymptotic behavior for large k is contained in Eq. (10.24). In this case the behavior for small ζ is most easily obtained from the second form in Eq. (10.14) and is

$$\frac{b^3 W_\perp(\zeta)}{Z_0} \to \frac{2b^{1/2}B}{\pi}\int_0^\infty \frac{dk}{k^{1/2}}\sin k\zeta = B\sqrt{\frac{2b}{\pi\zeta}}. \tag{10.28}$$

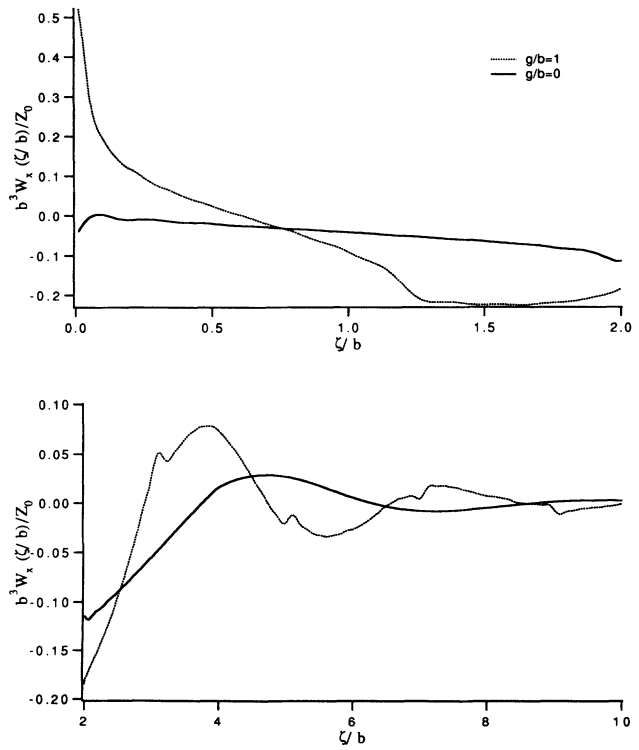

FIG. 11. Transverse wake function in units of Z_0/b^3 for $a/b = 100$ and $g/b = 0$ and 1.

We have used our numerical results for $Z'_\parallel(k)$ and $Z_\perp(k)$ to obtain the longitudinal and transverse wake functions using Eqs. (10.7) and (10.14). These are shown in Figs. 10 and 11 for $a/b = 100$ and $g/b = 0, 1$. Similar results can be obtained for other values of g/b if needed.

XI. SUMMARY

We consider the fields generated by a point charge traveling at $v \cong c$ near the axis of a beam pipe of constant cross section which contains an iris or collimator of constant cross section and length g. Using standard field matching techniques with appropriate boundary conditions we derive an integral equation [Eqs. (2.26) and (2.27)] for the tranverse electric field at the two junctions of the iris and the beam pipe. Both the longitudinal and transverse coupling impedances are then written in terms of this electric field [Eqs. (3.18) and (3.20)]. By judicious manipulation of the integral equation we are able to write a variational form for both the longitudinal and transverse impedance, with the trial function being the transverse electric field at the interface between the iris and the beam pipe.

We then specialize our analysis to a circular iris of radius b in a beam pipe of circular cross section of radius a and expand the trial function into a complete set of functions of r and θ satisfying the appropriate boundary conditions in the iris region. The variational format leads to extremely rapid convergence of the numerical calculations – in fact, we get results acurate to $\pm 1\%$ with only a few terms in the expansion. Numerical results are presented for $g/b = 1$ and $a/b = 2$, 5, 10, 100, and 1000.

Our interest in high values of a/b is directed toward expanding on earlier results for a hole in a plate of zero thickness [8]. In this work an expression is obtained for the longitudinal impedance as a function of $\gamma = (1-\beta^2)^{-1/2}$, the relativistic factor, for values of $kb \leq 1$. Of particular concern is that this expression diverges as $\gamma \to \infty$, a result we confirm for $\beta = 1$ when we let $a \to \infty$. But we have subtracted the term $(1/\pi)(b/a)$ from $Z_\parallel(k)/Z_0$ in Eqs. (8.1) and (8.2) and present well convergent result for the difference. Moreover we give complete results for both the real and imaginary parts of the longitudinal impedance for finite g/b and a/b. In addition we give the corresponding results for the transverse impedance where the divergence is no longer present. Of particular interest is $G(k)$, the "explicit" term in the impedance in Eqs. (3.18) and (3.19) which is readily evaluated for the longitudinal impedance in Eq. (6.6) and for the transverse impedance in Eq. (7.10).

The explicit term for the longitudinal impedance

$$R'_\parallel(k)\Big|_{\text{explicit}} \equiv \frac{1}{2\pi^2}G_\parallel(k) - \frac{1}{\pi}\ln\frac{a}{b} \tag{11.1}$$

is plotted separately in Fig. 1 and the explicit term for the transverse impedance

$$bR_{\text{explicit}}(k) = \frac{b}{2\pi^2 k}G_\perp(k) \tag{11.2}$$

is plotted separately in Fig. 5. As can be seen in these

figures, the explicit term, which is independent of g/b, captures the main features of the correct result and is accurate to approximately $\pm 50\%$.

Finally we examine the causality relations which apply for $\gamma \to \infty$ and obtain sum rules and asymptotic behavior of both the real and imaginary parts of the impedance for $k \to 0$, $k \to \infty$. These are then used to calculate the wake functions which are exhibited in Figs. 10 and 11.

ACKNOWLEDGMENT

This work was supported in part by the U.S. Department of Energy.

APPENDIX

The orthonormal modes $\boldsymbol{e}_n$ and $\boldsymbol{e}_\nu$ can be derived from the scalar functions satisfying the Helmholtz equation. In the pipe region we have

$$\nabla_\perp^2 \begin{Bmatrix} \phi_n \\ \psi_n \end{Bmatrix} = (\beta_n^2 - k^2) \begin{Bmatrix} \phi_n \\ \psi_n \end{Bmatrix}, \tag{A1}$$

while in the iris hole region

$$\nabla_\perp^2 \begin{Bmatrix} \phi_\nu \\ \psi_\nu \end{Bmatrix} = (\beta_\nu^2 - k^2) \begin{Bmatrix} \phi_\nu \\ \psi_\nu \end{Bmatrix}. \tag{A2}$$

Here we use the symbol ϕ to denote TM modes and the symbol ψ for TE modes. The boundary conditions for these potentials are given as follows:

$$\phi_n = 0 \quad \frac{\partial \psi_n}{\partial n_p} = 0 \text{ on the beam pipe surface } C_p, \tag{A3}$$

$$\phi_\nu = 0 \quad \frac{\partial \psi_\nu}{\partial n_h} = 0 \text{ on the iris hole surface } C_h, \tag{A4}$$

where $\partial/\partial n_p$ and $\partial/\partial n_h$ denote the differentiations in the normal directions, respectively, on the beam pipe surface and on the iris hole surface. The electric field in these modes is written as

$$\boldsymbol{e}_n = \begin{cases} -\nabla \phi_n & \text{for TM modes} \\ \boldsymbol{z} \times \nabla \psi_n & \text{for TE modes,} \end{cases} \tag{A5}$$

$$\boldsymbol{e}_\nu = \begin{cases} -\nabla \phi_\nu & \text{for TM modes} \\ \boldsymbol{z} \times \nabla \psi_\nu & \text{for TE modes.} \end{cases} \tag{A6}$$

Let us first try to simplify the integral in Eq. (3.12):

$$F_\nu \equiv \oint_{C_h} d\ell\, \boldsymbol{n}_h \cdot (\nabla \chi \times \boldsymbol{z}) \boldsymbol{z} \cdot (\nabla \times \boldsymbol{e}_\nu). \tag{A7}$$

Since $\boldsymbol{\nabla} \times \boldsymbol{\nabla} \phi_\nu = 0$, this integral vanishes for TM modes. Substitution of Eq. (A6) into Eq. (A7) leads to

$$F_\nu = (\beta_\nu^2 - k^2) \kappa_\nu, \tag{A8}$$

where we have used Eq. (A2), defining

$$\kappa_\nu \equiv \oint_{C_h} d\ell\, \boldsymbol{n}_h \cdot (\nabla \chi \times \boldsymbol{z}) \psi_\nu. \tag{A9}$$

Introducing the integral

$$\alpha_\nu \equiv \int_{S_1} dS\, \nabla \cdot \{\psi_\nu [\boldsymbol{z} \times \nabla (\sigma - \chi)]\} \tag{A10}$$

and noting that we consider here TE modes only, Eqs. (2.32) and (A6) give

$$\alpha_\nu = \zeta_\nu. \tag{A11}$$

On the other hand, applying the divergence theorem to Eq. (A10), we find

$$\begin{aligned} \alpha_\nu &= \oint_{C_h} d\ell\, \boldsymbol{n}_h \cdot [\boldsymbol{z} \times \nabla (\sigma - \chi)] \psi_\nu \\ &= \kappa_\nu + \oint_{C_h} d\ell\, \boldsymbol{n}_h \cdot (\boldsymbol{z} \times \nabla \sigma) \psi_\nu. \end{aligned} \tag{A12}$$

Since the term $\boldsymbol{z} \times \nabla \sigma$ is proportional to the source magnetic field within the iris hole, the second term on the right-hand side Eq. (A12) clearly vanishes. Thus, from Eq. (A11),

$$\kappa_\nu = \alpha_\nu = \zeta_\nu. \tag{A13}$$

Therefore, we obtain, from Eq. (A8),

$$F_\nu = (\beta_\nu^2 - k^2) \zeta_\nu. \tag{A14}$$

We now show that $\zeta_\nu = 0$ for TM modes. Substituting Eq. (A6) into Eq. (2.32), the TM mode contribution to ζ_ν is given by

$$\begin{aligned} \zeta_\nu = &- \oint_{C_h} d\ell\, \phi_\nu \frac{\partial}{\partial n_h} (\chi - \sigma) \\ &+ \int_{S_1} dS\, \phi_\nu \nabla^2 (\chi - \sigma), \end{aligned} \tag{A15}$$

where we have used Green's first identity. The first term on the right-hand side of Eq. (A15) vanishes because of the boundary condition (A4). In addition, since the source field potentials satisfy the Laplace equation, the second term is obviously zero. Thus

$$\zeta_\nu = 0 \quad \text{for TM modes.} \tag{A16}$$

In a similar manner we can show that $\xi_n = 0$ for TE modes. Substituting Eq. (A5) into Eq. (2.14) we have

$$\begin{aligned} \xi_n = &\int_{S_1} dS \left[\frac{\partial \psi_n}{\partial x} \frac{\partial (\sigma - \chi)}{\partial y} - \frac{\partial \psi_n}{\partial y} \frac{\partial (\sigma - \chi)}{\partial x} \right] \\ &- \int_{S_2} dS \left[\frac{\partial \psi_n}{\partial x} \frac{\partial \chi}{\partial y} - \frac{\partial \psi_n}{\partial y} \frac{\partial \chi}{\partial x} \right]. \end{aligned} \tag{A17}$$

Integration by parts leads to

$$\xi_n = - \oint_{C_h} d\ell\, (\sigma - \chi)_h \frac{\partial \psi_n}{\partial \ell} - \oint_{C_h} d\ell\, \chi_h \frac{\partial \psi_n}{\partial \ell}, \tag{A18}$$

where the subscript h corresponds to the iris hole surface. Here ℓ is the coordinate along the perimeter of the iris hole, and we have used the fact that $\chi = 0$ at the beam pipe surface. Since $\sigma = 0$ on the iris hole surface, we find that

$$\xi_n = 0 \quad \text{for TE modes.} \tag{A19}$$

[1] A. Chao, in *Physics of High Energy Particle Accelerators* (SLAC Summer School 1982), edited by Melvin Month, AIP Conf. Proc. No. 105 (AIP, New York, 1982), p. 353.
[2] R.L. Gluckstern and F. Neri, IEEE Trans. Nucl. Sci. **NS-32**, 2403 (1985).
[3] R.L. Gluckstern, J.B.J. van Zeijts, and B. Zotter, Phys. Rev. E **47**, 656 (1993).
[4] R.L. Gluckstern and J.A. Diamond, IEEE Trans. Microwave Theory Technol. **39**, 274 (1991).
[5] R.L. Gluckstern and S. Jiang (unpublished).
[6] S. Jiang, H. Okamoto, and R.L. Gluckstern (unpublished).
[7] Our definition of the transverse wake function is proportional to the transverse wake field produced by a source particle traveling off the axis. This is equivalent to the $m = 1$ longitudinal wake function of Chao [1], which is the derivative with respect to ζ of his transverse wake function.
[8] G. Dôme, E. Gianfelice, L. Palumbo, V.G. Vaccaro, and L. Verolino, Nuovo Cimento A **104**, 1241 (1991). This paper also contains references to earlier work (1959) by Dnestrovskii and Kostomarov on the radiation emitted when a charged particle beam passes through a circular hole in a plane metallic screen.